

## Incoherent scattering of gamma rays by *K*-shell electrons\*

Guy C. Spitale<sup>†</sup>

*Lawrence Livermore Laboratory, Livermore, California 94550*

Stewart D. Bloom

*Department of Applied Science, Lawrence Livermore Laboratory, Livermore, California 94550*

(Received 4 November 1976)

Differential cross sections for incoherent scattering by *K*-shell electrons have been measured, using coincidence techniques, for incident photons having energies of 662, 320, and 145 keV. Observations were made of the spectral distributions of scattered photons emerging at scattering angles ranging from 20° to approximately 140°. Target materials were iron, tin, holmium, and gold at 320 keV; tin and gold at 662 keV; and iron and tin at 145 keV. A typical spectrum generally displays a scattered quasi-Compton peak which is usually much narrower than would be expected from the bound-state electron motion. Rather than monotonically increasing with atomic number, the peak width typically reaches a broad maximum between  $Z = 50$  and  $Z = 67$  and then decreases with increasing atomic number. The peak, also typically, reaches a broad maximum width for scattering angles between 45° and 60°. No Compton defect is observed to within  $\pm 20$  keV. Underlying the quasi-Compton peak is a continuum which diverges at the low end of the scattered-photon spectrum for the following cases: gold, holmium, and tin targets for 320-keV incident photons; gold and possibly tin targets for 662-keV incident photons. This infrared divergence (IRD) is expected on general grounds and has been predicted. The observed IRD continuum is very nearly isotropic.

### I. INTRODUCTION

In this work we present experimental results on inelastic scattering from the *K* shell of four targets ranging in  $Z$  from 26 (Fe) to 79 (Au). Three incident photon energies were used, 145, 320, and 662 keV, although not all incident photon energies were used on all targets, due to experimental limitations which are described below. The measurements were all differential in both energy and angle, and were derived from energy spectra taken between appropriate energy limits (see below) at seven angles of scattering ranging from 20° to about 140°. Except at forward angles a quasi-Compton peak could be observed, by which is meant a broadened peak at the free Compton energy. The excluded angles were such that the binding-energy loss put the Compton peak beyond the spectrum cutoff at forward angles. Angles greater than  $\approx 140^\circ$  were excluded because of experimental limitations. In addition to the quasi-Compton peak a continuous spectrum rising towards low energies with a roughly  $1/k$  dependence was also observed, most clearly in the case of the 320-keV data. This continuous part of the spectrum can be identified with the expected IRD (infrared divergence).<sup>1,2</sup>

The IRD in incoherent scattering does not appear to have been studied in any published theoretical work prior to Ref. 1 and experimentally it appears the present work is the first instance of its explicit observation. As will be seen it can constitute a rather important part of the cross section de-

pending on the scattering angle and the lower-energy limit of the detector. In this work the presentation of results will emphasize the quasi-Compton peak when it was experimentally observable. Our principal (though not our only) concern with the IRD in this paper is with reference to the attendant error due to the inclusion of its tail, which underlies the quasi-Compton peak. This is discussed in Sec. III.

Among the effects noted in the present work was a lowering of the forward-scattering cross section as compared to the free-scattering Klein-Nishina prediction. This effect has been predicted in several incoherent-factor and form-factor theories.<sup>3,4,5</sup> In addition, the present work showed a few other qualitative features hitherto unpredicted and unobserved such as a relative insensitivity of the broadening of the quasi-Compton peak to scattering angle (in some instances) and also a somewhat anomalous dependence of this same broadening on the  $Z$  of the target. In addition, both of these effects showed a relatively strong dependence on the incident photon energy. These matters are discussed in more detail in the following sections.

There have been a number of experiments reporting the differential cross sections for Compton scattering by the *K* shell in targets of atomic number varying between 50 and 82.<sup>6-14</sup> The techniques used in most of these experiments<sup>6-11,14</sup> are essentially identical. When a gamma ray is scattered incoherently by an electron in the *K* shell, the electron is usually ejected from the atom leaving it in an excited (and ionized) state. The atom

decays by emission of a characteristic  $K$  x ray with a probability defined by the  $K$ -shell fluorescence yield. Photons scattered by the  $K$  shell can be distinguished from other scattered photons by demanding a coincidence with accompanying  $K$  x rays. This not only excludes from measurement photons scattered by other shells, but also coherently scattered photons, since these latter do not leave an excited atom. Nearly all experiments of this character used the 662-keV line of  $^{137}\text{Cs}$  as a source of incident gamma rays.

The present work was motivated in part by a desire to investigate the effects of electron binding on the differential cross sections in energy regimes lower than 662 keV because these regimes are, practically speaking, rather common. Also, valid comparisons with theory, though not now possible, may well be possible in the near future. Chintalapudi and Parthasarathi<sup>11</sup> also reported measurements for 320-keV photons incident on Pb, Ta, and Sm at angles between  $30^\circ$  and  $130^\circ$ . However, their results were in disagreement with data presented by Pingot<sup>13</sup> for 279-keV photons incident on Ta and Sm at angles between  $70^\circ$  and  $160^\circ$ . It was our further hope to resolve this conflict, if possible, by studying the dependence of the cross section on energy. The integrated cross section could depend strongly on the low-energy cutoff, where the IRD might play an important role. We feel it is reasonable in fact to attribute the discrepancy between Refs. 11 and 13 to differing low-energy thresholds of the respective detection systems. In addition, in the present work the experimental apparatus was generally capable of resolving the quasi-Compton peak due to its sharpness. Thus we were able (in general) to characterize the behavior of the width and position of the Compton peak as a function of scattering angle, atomic number, and source energy.

## II. EXPERIMENTAL PROCEDURE

### A. Targets and sources

The matrix of targets and sources is listed in Table I. Four elementary targets were used: iron ( $Z=26$ ), tin ( $Z=50$ ), holmium ( $Z=67$ ), and gold ( $Z=79$ ). The gold targets used at 145 and 320 keV actually consisted of a copper-gold alloy (10% Au-90% Cu by number). At 662 keV only gold and tin were studied and only tin at 145 keV. See Sec. IID for a discussion of these limitations.

### B. Method

The experimental method used is shown schematically in Fig. 1. The target foil was viewed by two detectors; one was sensitive to characteristic

TABLE I. Summary of targets, sources, and target thicknesses.

Source	$E_\gamma$ (keV)	$Z$	Angle of scatter (deg)	Thickness (mg/cm <sup>2</sup> )
$\text{Cs}^{137}$	662	79 <sup>a</sup>	20-138	26.6, 135, 192
$\text{Cs}^{137}$	662	79	20-142.3	17.0, 108, 262
$\text{Cs}^{137}$	662	50	20-142	19.6, 62.2
$\text{Cr}^{51}$	320	79 <sup>a</sup>	20-137.4	26.6, 135, 192
$\text{Cr}^{51}$	320	67	20-136	21.9
$\text{Cr}^{51}$	320	50	20-136	19.56, 62.2
$\text{Cr}^{51}$	320	26	20-137	15.8
$\text{Ce}^{141}$	145	26	20-137	15.8

<sup>a</sup>Solid suspension of 75% copper, 25% gold by weight.

$K$  x rays emitted by the target and the other to scattered gamma rays. The signals from these detectors were processed electronically by a slow-fast coincidence circuit.<sup>15</sup> The lower discriminator settings for the scattered gamma are shown in Table II. The coincidence window was 15-20-nsec wide. The records of the accepted events were stored in a multichannel analyzer which sorted them as a function of energy (pulse height). The differential scattering cross section was determined from the effective source strength, target fluorescence yield, detector efficiencies, and solid angles subtended by both detectors. The data were corrected for a number of effects to be discussed below.

As shown in Fig. 1 the source and associated shielding rested on a stationary platform. Targets were mounted several centimeters in front of the source slit in such a way that the polar and azimuthal tilt angles could be adjusted. The gamma-ray detector rested on a surface which could be swiveled about the central axis of the target. The

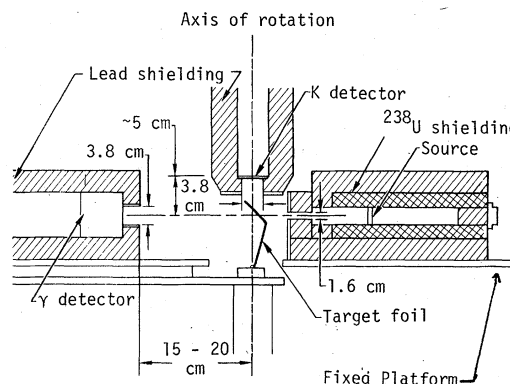


FIG. 1. Schematic diagram of experimental apparatus. The scattering angle is adjusted by rotating the table supporting the gamma detector about an axis passing vertically through the center of  $K$  x-ray detector. See Sec. II for further details.

x-ray detector was stationed directly above and looking down on the target.

### C. Detector efficiencies

Sodium iodide scintillation detectors were selected for both legs of the coincidence system because of their high efficiency and relatively simple operating characteristics. The Compton detector was 7.62 cm long by 7.62 cm in diameter and the  $K$  x-ray detector was 0.32 cm thick by 5.08 cm in diameter. Both detectors were collimated down to a diameter of 3.8 cm for the purpose of minimizing escape effects.

The overall efficiency of the gamma-ray detector was determined by use of calibrated sources and found to be 100% over the energy range of interest for the full spectrum. The photopeak efficiency was not 100% over the same energy range. This point is discussed in more detail in Sec. II E.

### D. Background suppression

In order to minimize the rate of accidental counts, several precautions were taken. Both detectors were surrounded by 1-in. thicknesses of lead except, of course, for the required apertures. The radioactive sources were imbedded in a 10-cm cube of depleted  $^{238}\text{U}$ . This cube was, in turn, surrounded by a 5-cm thickness of lead. Additional movable lead shielding was used to prevent the gamma-ray detector from directly viewing the source slit in various arrangements depending on angle of scatter. The  $K$  x-ray detector was always located so that it was not exposed to scattered radiation from the source slit. All lead surfaces in the field of view of the gamma-ray detector were covered by a graded- $Z$  absorber designed to suppress characteristic lead x rays. This absorber consisted of the following (starting from the wall): 30 mil or 0.76 mm of cadmium, 10 mil or 0.25 mm

TABLE II. Limits on experimental energy windows.  $E_s$  is the source energy and  $E_B(Z)$  the  $K$ -shell binding energy. The upper discriminator was always set well above the energy limit,  $E_s - E_B(Z)$ ; see column 4.

$E_s$ (keV)	$Z$	Experimental lower threshold (keV)	$E_s - E_B(Z)$ (keV)
662	79	160	582
662	50	60	633
320	79	30	240
320	67	80	265
320	50	50	29
320	26	45	313
145	26	20	138

of copper, and 10 mil or 0.25 mm of aluminum.

Further precautions were necessary because of the spurious or so-called "false" coincidence count rate. The possible causes of these coincidences are fairly numerous. However, the most important single cause is the photo-electrons which may emit bremsstrahlung photons and/or ionize other atoms, resulting, for example, in the emission of additional  $K$  x rays. Both of these are second-order effects which cause a spurious peak to appear at the  $K$  x-ray energy in some of the spectra.<sup>15</sup> Another result of these processes is the simultaneous detection of a  $K$  x ray by the  $K$  detector and a bremsstrahlung photon by the Compton detector. Spurious counts are also induced by the presence of products and by-products of other types of events, e.g., Compton scattering by other shells, coherent scattering, photoelectric absorption.

All the effects discussed above are caused by events which occur inside the target foil. The products and by-product of a scattering event may also interact with the surroundings of the target and detectors and, after multiple interactions, be counted by one of the detectors. Also a spurious count can be generated by a photon which fires either detector and scatters into the other. This cross talk was easily eliminated, however, by the simple artifice of insuring that neither detector was in the direct field of view of the other.

In general, the dependence on target thickness of that part of the spurious count rate produced by simultaneous detection of a direct product and a by-product of a scattering event will not be the same as that of the true count rate. The contribution to the measured count rate was therefore determined by taking measurements on targets of varying thickness in order to determine the magnitude of the thickness-dependent correction. In cases reported here the effect was well under 10%. The thickness-independent contribution to the background is due to multiple interactions of photons with the target surroundings and coincidences between Compton electrons and x rays of scattered photons. Its magnitude was determined by replacing the target with an equivalent thickness of aluminum or beryllium.

Since in most instances it was found that the "false" rate discussed above never exceeded 25% of the total count rate the contribution from this source to the statistical uncertainty was rather small. Also it is worth noting that our background was somewhat lower than the average reported in the literature (although East and Lewis<sup>10</sup> report a false rate of ~1%-2%). This is probably due to the use of graded- $Z$  absorbers and the fact that the coincidence windows used in this work were several orders of magnitude narrower than those used

in all preceding experiments except that of East and Lewis.<sup>10</sup> It was further noticed that placing an 8-mm plastic filter in front of the x-ray detector reduced the false rate to no more than 5% of the total measured rate. The thickness of this filter is greater than the range of 600-keV electrons. A reasonable conclusion would then be that most of the spurious count rate was due to coincidences between scattered (and detected) photons and Compton electrons.

#### E. True coincidence spectra

The raw experimental data were collected in the form of an array of counts vs channel number in a multichannel analyzer. The true count rate (for our purposes)  $C$  as a function of channel  $n$  is found by correcting for the accidental count rate  $C_a$ , the "false" rate  $C_f$ , and the false-accidental count rate  $C_{fa}$ , and is given by

$$C(n) = C_t(n) - C_a(n) - [C_f(n) - C_{fa}(n)] \quad (1)$$

The channel number was related to the scattered photon energy  $E_f$  by means of energy vs channel calibrations with known radioactive sources. A calibration curve was made each time the gain in the system was changed. The system was found to be linear to within the limits set by gamma ray detector resolution.

The transformation of the reduced count rate  $C(E_f)$  into the doubly differential cross section  $d\sigma/d\Omega dE_f$  is given by,

$$\frac{d\sigma_c}{d\Omega dE_f} = \frac{C(E_f)/\Delta E_f}{(2S\Omega_b/4\pi)(\epsilon_K\Omega_K/4\pi)\Omega_\gamma\omega_K G_c(E_f)\epsilon_\gamma(E_f)} \quad (2)$$

where  $S$  is the source strength in disintegrations per second,  $\Omega_b/4\pi$  is the relative solid angle subtended by the defining collimator with respect to the source,  $\Omega_K/4\pi$  is the relative solid angle subtended by the sensitive area of the  $K$  detector with respect to the irradiated area on the target,  $\Omega_\gamma$  is the absolute solid angle subtended by the sensitive area of the gamma detector with respect to the irradiated area on the target,  $\epsilon_\gamma(E_f)$  is the efficiency of the gamma-ray detector for energy  $E_f$ ,  $\omega_K$  is the  $K$ -shell fluorescence yield,  $G_c$  is the geometry dependent factor correcting for absorption within the target, and  $\Delta E_f$  is the energy width of a channel.

All of these quantities were readily ascertained. The factor  $S(\Omega_b/4\pi)\epsilon_K$  is actually the "effective" source strength determined by the source calibration procedure which will be discussed in Sec.

II F.  $\Omega_\gamma$  must be small (in this experiment less than 0.04 sr in all cases) in order to obtain rea-

sonably fine angular resolution. No such constraint influenced the placement of the  $K$  detector, and so  $\Omega_K/4\pi$  was maximized. A simple calculation which summed over small differential areas on the irradiated surface was done in order to determine  $\Omega_K/4\pi$ . The spectral response  $\epsilon_\gamma(E)$  was determined by using several monochromatic energy standards. Both radioactive sources and photons scattered by nearly free electrons (e.g., aluminum) were used for this measurement which showed that the Compton edge was relatively unimportant for photon energies less than 300 keV.<sup>15</sup> The dependence of the photoelectric escape peak on incident photon energy was found to adhere to the theoretical optimum described in Siegbahn's work.<sup>16</sup> The effect of photoelectric escape is negligible at energies greater than 100 keV.

As can be seen from the remarks above there is a regime over which the recorded spectra can be used without any spectral correction. This regime happens to coincide with that range of energies over which the Compton spectra generated by the 320-keV source are distributed. Accurate determinations of the spectra generated by the scattering of 662-keV photons would require that the measured spectra be mathematically unfolded in order to compensate for Compton escape processes, a difficult and unreliable procedure. The photoescape which distorts the spectra produced by the 145-keV source can be dealt with by making the reasonable assumption that the width of the escape peak was much less than the separation between the photo and escape peaks. The correction involved is negligible at incident energies above 100 keV but can be sizable below this limit. Because of these uncertainties only the Fe data was considered reliable in this case (145 keV)

#### F. Source calibration

The effective source strength depended not only on actual strength but also on such things as the solid angle subtended by the aperture in the source collimator, the photopeak efficiency of the x-ray detector, and the settings of the single-channel analyzers and amplifiers in the x-ray leg of the electronics. The calibration for the effective source strength was done by exposing the target to source radiation collimated as in the actual coincidence experiment. The effective source strength was then given by

$$S_0 = \frac{S_K}{(\Omega_K/4\pi)\sigma_p\omega_K G_K} \quad (3)$$

where  $S_K$  is the count rate of the x-ray detector,  $\Omega_K$  is the solid angle subtended by the x-ray detector,  $\sigma_p$  is the cross section for photoelectric

absorption of source photons,  $\omega_K$  is the  $K$ -shell fluorescent yield, and  $G_K$  is the correction for absorption in target.

### G. Self-absorption corrections

In addition to the thickness dependent spurious effects discussed in Sec. IID, the experimental value for  $d\sigma/dEd\Omega$  may be influenced by the attenuation of  $K$  x rays, scattered gamma rays, and source photons. Necessary self-absorption corrections were incorporated into  $G_c$  and  $G_K$  as used in Eqs. (2) and (3). Expressions for  $G_c$  and  $G_K$  are given in Ref. 15. It was found that only negligible corrections  $G_c$  and  $G_K$  were required in energy regions where the quasi-Compton peaks appeared. However, in the lower-energy portions of spectra wherein the IRD dominated the spectrum, significant corrections were required. In the worst cases (e.g., scattered photons of energies near 50 keV for 320-keV photons incident on gold or holmium) corrections of the order of 15% were required.

### III. RESULTS AND DISCUSSION

The results of our measurements are presented in Figs. 2-6 and Tables III-IV. In Figs. 2(a)-2(d) we give illustrative spectra for forward and backward scattering angles in the case of 662-keV photons incident on Au and 320-keV photons incident on Ho. Since all the spectra in Figs. 2(a)-2(d) have been corrected for background (see above), the continuum present in all these figures is largely attributable to the IRD (see below). It clearly contributes to the uncertainty in extracting the area under the quasi-Compton peak, particularly in Figs. 2(a), 2(c), and 2(d). In Fig. 2(b) on the other hand, the narrowness of the quasi-Compton peak (at 225 keV) makes the contribution of the IRD negligible. In Fig. 2(c) [320-keV photons incident on Ho ( $Z=67$ ),  $\theta=20^\circ$ ] the quasi-Compton peak is eliminated by the binding-energy requirement and the contribution of the IRD is paramount. In Fig. 2(d), the same as Fig. 2(c) except  $\theta=136^\circ$  rather than  $120^\circ$ , the quasi-Compton peak is available energetically, quite narrow, and quite evident. However, unlike Fig. 2(b), the contribution of the IRD is very comparable to the area under the peak. In this case the photon momentum transfer and the electron momenta (in the  $K$  shell) are in very much the same range,  $\approx 0.5-1.5$  in natural units ( $\hbar=c=m=1$ ), and the competitive nature of the cross sections for the IRD and the quasi-Compton scattering is to be expected.<sup>17</sup>

In all cases it is clear that the apparent cross section will depend on the lower discriminator setting such that the lower the setting the higher

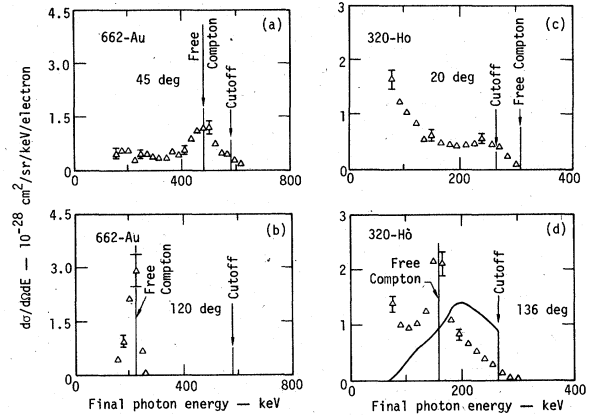


FIG. 2. Experimental results for the doubly differential ( $d^2\sigma/dE d\Omega$ ) scattering cross section vs final photon energy for four cases: (a) 662-keV photons incident on gold ( $Z=79$ ), scattering angle  $45^\circ$ . The free-scattering prediction (the long vertical line marked "free Compton") is 479 keV and the high-energy cutoff (shorter vertical line marked "cutoff") is 582 keV. The vertical bars (on all curves) represent the experimental error and are typical of all the points. (b) 662-keV photons incident on gold, scattering angle  $120^\circ$ . The free Compton and cutoff energies are 225 and 582 keV, respectively. (c) 320-keV photons incident on holmium ( $Z=67$ ), scattering angle  $20^\circ$ . The free Compton and cutoff energies are 308 and 265 keV, respectively. The main contribution to the spectrum here is the IRD. (d) 320-keV photons incident on holmium, scattering angle is  $136^\circ$ . The free Compton and cutoff energies are 155 and 265 keV, respectively. In this case we also show the prediction of the semiclassical theory by the solid line (see Sec. III). As in (c) the contribution of the IRD is the major contribution but in this case the quasi-Compton peak is energetically accessible and visible.

the calculated cross section. For the 320-keV data the situation is much more sensitive in this regard than for the 662-keV data, as might be expected, and the presence of the IRD (at 320 keV) in the Sn and Au data, not shown here, constitutes a large

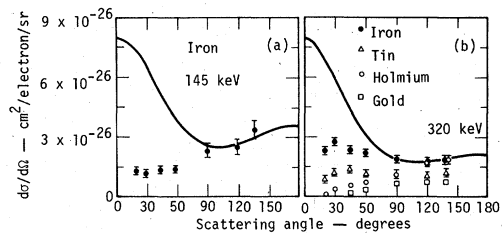


FIG. 3. Energy-integrated quasi-Compton peak cross sections as a function of angle for several cases: (a) 145-keV photons incident on iron ( $Z=26$ ). (b) 320-keV photons incident on iron ( $Z=26$ ), tin ( $Z=50$ ), holmium ( $Z=67$ ), and gold ( $Z=79$ ). The solid lines on both graphs represent the free-scattering (Klein-Nishina) prediction. The vertical bars are the experimental errors (missing when the errors are smaller than the point-symbols).

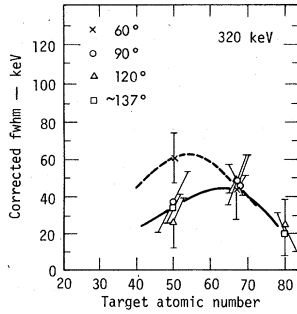


FIG. 4. Corrected fwhm (full width at half maximum) of quasi-Compton peak vs target atomic number for 320-keV photons incident (see Sec. III). The experimental errors are represented by vertical bars. The data for  $Z=26$  are not shown because of their very large uncertainty (see Table IV). The curves are intended to guide the eye only.

effect. Similar remarks pertain to the Sn data at 662 keV, also not shown here.

Because of the fact that, hitherto, the IRD in inelastic Compton scattering has not been observed (or identified) special pains were taken to eliminate all possible spurious sources which might account for the low-energy continuum. As noted in Sec. IID the main concern was the photoelectrons ejected from the  $K$  shell which lead to bremsstrahlung photons which would be in actual coincidence with characteristic  $K$  x rays. This would be a source of "false" coincidences which one could not distinguish from "true" coincidences by repeating the experiment using an aluminum tar-

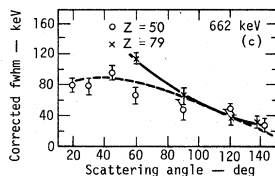
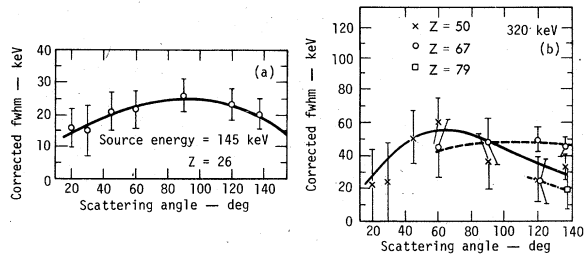


FIG. 5. Corrected fwhm of quasi-Compton peak vs scattering angle for (a) 145-keV photons incident on Fe ( $Z=26$ ), (b) 320-keV photons incident on Au ( $Z=79$ ), Ho ( $Z=67$ ), and Sn ( $Z=50$ ), (c) 662-keV photons incident on Sn ( $Z=50$ ) and Au ( $Z=79$ ). The curves are intended to guide the eye only. The vertical bars represent the experimental errors.

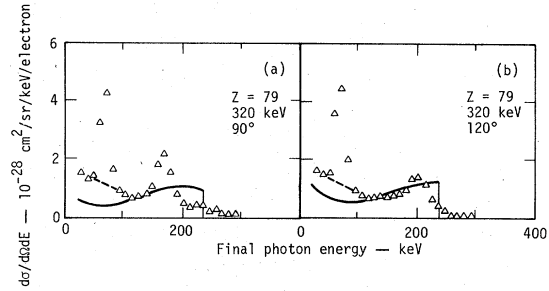


FIG. 6. Theoretical prediction (solid line, Ref. 2) compared to experimental results for  $d\sigma/d\Omega dE$  for 320-keV photons incident on Au ( $Z=79$ ) at two angles: (a)  $120^\circ$ , (b)  $90^\circ$ . The experimental errors (not shown) are roughly the size of the triangular points. The peak at 70 keV is due to spurious coincidences between gold x-rays detected in the gamma detector and scattered photons detected in the  $K$  detector (see Fig. 1).

get. This contribution would resemble our observed IRD, qualitatively, in both spectrum and angular distribution. Since photoelectrons would initially carry an energy equal to the source energy minus the target  $K$ -shell binding energy, the corresponding bremsstrahlung spectrum would consist of a divergence with a cutoff at the maximum electron energy. This would be identical to that of our observed IRD. Since photoelectrons are emitted isotropically in the CM (center-of-mass) and LAB (laboratory) frames from high- $Z$  target atoms are practically identical, one would expect the resulting bremsstrahlung to be isotropically distributed. We see some anisotropy ( $\approx 10\%$ ) in the IRD in our experimental data, but not to such a degree that bremsstrahlung could be eliminated as a possible cause of the observed IRD without further considerations.

Although Shimizu *et al.*<sup>9</sup> estimated this effect to constitute a negligible contribution to their observed cross sections, we undertook an independent estimate. Using the expressions given by

TABLE III. Width of quasi-Compton peak for 145-keV incident. Only the Fe data was usable in this case (see Sec. II).

$\theta_s$ (deg)	Corrected fwhm (keV)
20	$16 \pm 6$
30	$15 \pm 8$
45	$21 \pm 6$
60	$22 \pm 6$
90	$26 \pm 5$
120	$23 \pm 5$
137.4	$20 \pm 5$

TABLE IV. Width of quasi-Compton peak for 320-keV incident.

$\theta_s$ (deg)	Corrected fwhm (keV) $Z=79$	Corrected fwhm (keV) $Z=67$	Corrected fwhm (keV) $Z=50$	Corrected fwhm (keV) $Z=26$
20	a	a	22 ± 22	23 ± 22
30	a	49 <sup>b</sup>	24 ± 24	25 ± 25
45	a	52 <sup>b</sup>	51 ± 16	35 ± 15
60	a	45 ± 18	61 ± 14	38 ± 12
90	26 <sup>b</sup>	49 ± 14	37 ± 17	22 ± 14
120	25 ± 14	50 ± 8	26 ± 14	24 ± 9
136		46 ± 6	34 ± 8	
137				17 ± 8
137.4	20 ± 12			

<sup>a</sup> Peak suppressed by energy conservation condition.

<sup>b</sup> Peak eroded by energy conservation condition.

Heitler,<sup>18</sup> we estimated the radiation length of Compton electrons of energies concerned in cases which exhibited strong IRD and found these to be of the order of  $10^5$  mg/cm<sup>2</sup> which is to be compared with foil thickness of approximately 20 mg/cm<sup>2</sup>. On the basis of this result we estimate that not more than 0.02% of the *K*-shell electrons emitted produced bremsstrahlung photons. This is in rough agreement with the estimate of Shimizu *et al.*<sup>9</sup> that the size of the effect was not more than 0.1% for their experiments. This is to be contrasted with an observed IRD of magnitude greater than ten times the area under the quasi-Compton peak, as can be seen for example in Figs. 2(c) and 2(d).

We then turned our attention to coincidences between bremsstrahlung photons and *K* x rays emitted by atoms excited by electrons freed by photoelectric events. Although this is a higher-order effect, the presence of great numbers of photoelectrons makes it a possible cause of bremsstrahlung background. Using a procedure similar to that described above, we estimated that this effect would produce a bremsstrahlung background

of no more than 0.8% of the quasi-Compton peak. Although there may be numerous other processes which may result in coincidences between bremsstrahlung and *K* x rays, they are all of higher order than the processes considered above, and thus can be disregarded.

Finally, experimental verification of the foregoing analysis was sought. Our measurements indicate that, for the target thicknesses utilized in the present work, the bremsstrahlung background counts were well below 10% of the total counts in the IRD region or the quasi-Compton peak. In particular, we compared spectra produced by gold targets of thickness 200, 100, and 20 mg/cm<sup>2</sup> for source energies of 662 and 320 keV at several scattering angles. We also examined spectra produced by target foils composed of an alloy of copper and gold (25% gold and 75% copper by weight) under the same experimental conditions. Besides the essentially unobservable change in count-rate per mg thickness, we also note that within ±10%, no difference of the relative magnitude of the observed IRD compared to the quasi-Compton peak was observed. This confirms the relatively background-free character of our IRD spectra. However, it is worth noting that for such a high-*Z* target as gold the smallness of the IRD compared to the quasi-Compton peak [see Fig. 2(a)] makes it difficult to extract a good value for the cross section of the IRD. It is clear (for the present) that the best data for this purpose is Ho; see Figs. 2(c) and 2(d) and the following discussion.

A rough estimate can be made of the IRD cross section using the approach of Heitler in the calculation of the production of bremsstrahlung.<sup>18</sup> In this case we combine the photoelectric cross section with the appropriate second-order correction which then leads to the IRD cross section. In doing this the assumption is made that the IRD is angularly isotropic. The crude approximation that results is

TABLE V. Width of quasi-Compton peak for 662-keV incident.

$\theta_s$ (deg)	Corrected fwhm (keV) $Z=79$	Corrected fwhm (keV) $Z=50$
20	a	78 ± 9
30	a	77 ± 12
45	106 <sup>b</sup>	95 ± 10
60	115 ± 8	66 ± 13
90	66 ± 11	49 ± 14
120	40 ± 10	50 ± 14
137	34 ± 8	
142		30 ± 9

<sup>a</sup> Peak suppressed by energy conservation condition.

<sup>b</sup> Peak eroded by energy conservation condition.

$$\frac{d^3\sigma_c}{d\Omega dE_f} \approx \frac{\alpha}{\pi} \frac{\sigma_{pe}}{4\pi E_f}, \quad (4)$$

where  $E_f$  is the final photon energy,  $\sigma_{pe}$  is the appropriate photoelectric cross section (both energy and  $Z$  dependent), and  $\alpha$  is the fine-structure constant. The factor  $\alpha/\pi$  is part of the second-order correction to the photoelectric effect, which the observed IRD in the inelastic Compton scattering must exactly equal in magnitude and energy ( $E_f$ ) dependence. This argument is precisely the same as applies to the cancelling second-order corrections in each of the two phenomena, Coulomb scattering, and bremsstrahlung.<sup>18</sup>

Applying Eq. (4) to the best case for our purposes, namely the scattering of 320-keV photons from Ho,  $Z=67$  [see Figs. 2(c) and 2(d)], we find that the ratio of the observed doubly differential cross section to that predicted by Eq. (4) is in the range  $1.0 \pm 0.5$ . The energy range and angular range used to obtain this result were 45–90 keV and  $20^\circ$ – $136^\circ$ , respectively. In view of the very rough nature of Eq. (4), the agreement even to within a factor of two must be in part fortuitous. What cannot be fortuitous, however, is the order of magnitude of the predicted IRD. It is unlikely to be negligible in this case.

In Figs. 3(a) and 3(b) we show the dependence on angle of the cross section for the quasi-Compton scattering at two energies, 145 keV [Fig. 3(a)] and 320 keV [Fig. 3(b)]. At 145 keV, only the data for the lightest target (Fe) was usable (see Sec. II). In both cases the fall-off at forward angles compared to the Klein-Nishina (free-electron) prediction is quite evident. Such a fall-off is to be expected from a simple semiclassical model which uses the Klein-Nishina formula in conjunction with the expected momentum distribution of the  $K$ -shell electrons.<sup>19</sup> Such a model was employed by Motz and Missoni<sup>14</sup> and we have used essentially the same model to make similar calculations in order to understand, at least qualitatively, the results in Figs. 3(a) and 3(b) (and also the following figures).<sup>17</sup> Our calculations show that at forward angles, only that portion of the electron momentum distribution which is both large in magnitude compared to the average magnitude and antiparallel in direction to the incident photon direction will contribute to the inelastic scattering. This double limitation produces a much reduced cross section in consonance with the findings in Ref. 14. However, since the model neglects, among other things, the Coulomb scattering in the intermediate state (after absorption of the incident photon) it tends to under-predict the forward scattering. Thus, for one example, the cross section cannot be expected to disappear at  $0^\circ$ , even using the

semiclassical model, although it will be much smaller than the free-electron prediction of course, as was found experimentally. Two other failures of the semiclassical model are its inability to correctly deal with the Compton shift (see below) and, of course, the total absence of an IRD. Both of these failures are due to the completely elastic character of the calculation and are to be expected. A good example illustrating these matters is the scattering of 320-keV photons from Ho ( $Z=67$ ), as shown in Fig. 2(d).

At back angles ( $\theta > 90^\circ$ ) the observed cross section for 320-keV photons is significantly smaller than the free Klein-Nishina prediction, by a factor of up to two [see Fig. 3(b)], whereas at 145 keV there is good agreement, as shown in Fig. 3(a). Our semiclassical calculations at 320 keV (not shown) show a *decrease* at back angles (compared to the Klein-Nishina prediction) as well as a (relative) *increase* at these same back angles at 660 keV. (The 660-keV data and semiclassical calculations of Ref. 14 are in excellent agreement with our calculations, as might be expected.) However, the relative behavior in Fig. 3(b) of the experimental points for Ho ( $Z=67$ ) and Sn ( $Z=50$ ) are not reproducible by our semiclassical calculations. In the experimental data the former is essentially at the Klein-Nishina limit while the latter is down by a factor of  $1/2$  for  $\theta \geq 120^\circ$ , while our calculations show an even bigger decrease at  $Z=67$  than at  $Z=50$ .

In Figs. 4, 5(a), 5(b), and 5(c) are plotted our experimental results for the corrected fwhm (full-width at half-maximum) of the quasi-Compton peak. The method of correction is discussed in Ref. 15. The results are given numerically in Tables III–V. The results of Figs. 4, 5(a), and 5(b) are consistent with an angularly independent fwhm (to within a factor of two) but a highly  $Z$ -dependent behavior, for 320-keV incident photons. The peaking of the fwhm around  $Z=50$  to  $Z=67$  (see Fig. 4) is clear. (We do not show the low- $Z$  results where the fwhm is zero for all practical purposes.) Neither the relative angular behavior or the absolute values of the fwhm values in Fig. 5(c) (662-keV incident on targets of  $Z=50$  and  $Z=79$ ) are predicted correctly by the semiclassical model, the results of which we do not show here. The results of the semiclassical calculation not only require much broader peaks (by a factor of 2 or more) but an increase of the fwhm with scattering angle, as might be expected from purely classical considerations. See Fig. 2(d) for an example of the semiclassical prediction and its comparison with experiment.

In Figs. 6(a) and 6(b) we show a comparison between our experimental results and the relativistic

calculation of Wittwer<sup>2</sup> for an incident photon energy of 320 keV and a gold target,  $Z=79$ . This calculation was truncated to include only dipole and quadrupole emission and absorption. It is not surprising therefore that the Compton peak is practically undiscernible in the theoretical curve of Fig. 6(a) ( $\theta=120^\circ$ ). However, the quantitative agreement for cross sections averaged over  $\approx 100$ -keV intervals is really quite good, excluding the spurious peak at 70 keV, of course (see Sec. II). This same spurious peak obscures the IRD in the experimental data, and so it is not possible to say very much concerning the comparison of theory and experiment in the low-energy region. As already noted, however, the theoretical calculation does continue to rise (towards  $E_f=0$ ) with a  $1/E_f$  dependence in the low-energy region (see Refs. 1, 2).

We reserve to the last the discussion of the apparent lack of any Compton defect in the centroids of all the quasi-Compton peaks which could be located with any precision. In no case was the change from the expected free-scattering energy greater than 20 keV and in some cases the statistics permitted an upper limit of  $\lesssim 10$  keV. If we were to use the well-known low-energy prediction for a shift in wavelength ( $\lambda$ ) this would correspond to a wavelength change ( $\Delta\lambda$ ) of the order of  $|\epsilon_k|/k^2$ ,<sup>20,21</sup> where  $|\epsilon_k|$  and  $k$  are the  $K$ -shell binding energy and incident photon wave number, respectively, in natural units (see above). In the case of 662-keV photons incident on a gold target ( $Z=79$ ) this would amount to a downward shift in the scattered energy of  $\approx 50$  keV. In Appendix A we present a short resume of earlier Compton-shift formulas and a few calculated results for the centroid shift based on the semiclassical model, wherein the elastic limitation as well as the low-energy approximations are lifted. For all the cases reported here the application of the results of Appendix A lead to the prediction that the energy shift will be  $\lesssim 5$  keV, and not necessarily in the downward direction. In any case, this limit is at least a factor of two beyond the precision with which we can ascertain the centroid position in our experimental results. It thus appears that the semiclassical model can be successfully applied to the average energetics pertaining to the Compton process. Furthermore it yields the same results, regardless of whether the process is inelastic or not. However, beyond this its usefulness is rather limited as described above.

#### ACKNOWLEDGMENT

The authors would like to thank Rex Booth and K. J. Tirsell for technical assistance and advice. We would also like to express our appreciation to

Dr. Leon Wittwer for making available the results of his theoretical calculation.

#### APPENDIX: THE COMPTON DEFECT

The existence of a "Compton defect," i.e., a shift towards a longer wavelength for the scattering of photons (from bound electrons) than the free-electron prediction, has been known for more than forty years. The phenomenon was shown to be a binding-energy effect in 1934 by Bloch<sup>20</sup> in what we call the low-energy limit (see below). A review of similar theoretical treatments as well as measurements (up until 1955) was given by Evans.<sup>21</sup> In this appendix we give some results on the Compton defect based on the semiclassical model described in Sec. III and in Ref. 14, with the addition that the inelastic character of the process is included in the kinematics. Our considerations are limited to  $K$ -shell inelastic scattering and our purpose is to discover what happens in more general situations than the low-energy limit. Such situations would include all the cases which form the subject matter of the present work, wherein the photon and electron momenta are not only comparable but the latter is relativistic (as well as the former). Using momentum and energy conservation the following formulas can be derived with one principal assumption, which we will shortly describe:

$$k' = \frac{f_1 k}{f_2 + k(1 - \cos\theta)}, \quad (A1)$$

$$f_1 = \frac{(k + \epsilon_0)(2 + k + \epsilon_0) - \langle p \rangle^2}{2\langle p \rangle}, \quad (A2)$$

$$f_2 = \frac{k(1 + k + \epsilon_0 - \langle p \rangle)}{\langle p \rangle}, \quad (A3)$$

where we have used natural units ( $\hbar=m=c=1$ ) and  $k$  is the initial photon energy,  $k'$  the final photon energy,  $\theta$  the photon scattering angle,  $-\epsilon_0$  the initial  $K$ -shell electron binding energy  $\approx Z^2\alpha^2/2$ , and  $\langle p \rangle$  is the average magnitude of  $p$ , the initial total "microscopic" momentum; i.e., the magnitude of the vector sum of the initial photon momentum and the electron momentum averaged over all the directions and magnitudes characterizing the  $K$ -shell distribution. The results Eqs. (A1)–(A3) are based principally on the assumption that the replacement of  $\langle p \rangle$  with  $p$  in Eqs. (A1)–(A3) plus subsequent averaging over all  $p$  (see above definition of  $\langle p \rangle$ ), will lead to the same result for  $k'$ .

The low-energy limit of Eqs. (A1)–(A3) is easily defined and calculated:

*Low-energy limit:*  $|\epsilon_0| \ll k \ll 1$ ,

$$\Delta\lambda \equiv \lambda' - \lambda \approx (1 - \cos\theta) \left( 1 - \frac{|\epsilon_0|}{2k^2} \right) + \frac{5}{4} \frac{|\epsilon_0|}{k^2}, \quad (A4)$$

where  $(\lambda, \lambda')$  are the (initial, final) wavelengths in natural units. If we neglect the departure from unity in the correction factor multiplying the angular term  $(1 - \cos\theta)$ , the result is essentially the same as the correction  $(\lambda)^2|\epsilon_0|$  derived by Bloch and others.<sup>19,20</sup> The neglect of the correction to  $(1 - \cos\theta)$ , however, is justifiable only when  $(\lambda)^2|\epsilon_0|$  is  $\ll 1$  and/or  $\cos\theta \approx 1$  (forward angles).

The next case we treat is more general in that only the energy of the photon is restricted so that its momentum will be large compared to that of the initial electron. In this case Eqs. (A1)–(A3) yield the following:

*Low-Z limit:*  $Z\alpha \ll k$ ,

$$\Delta\lambda \approx (1 - \cos\theta)(1 + |\epsilon_0|). \quad (\text{A5})$$

The change between Eqs. (A4) and (A5) is very

notable; the Compton defect has become (for most purposes) very much smaller, relative to the incident wavelength. This result is in keeping with the experimental findings in the present work. However, in order to check this finding more closely the functions  $f_1$  and  $f_2$  were evaluated in the specific cases which were studied here (see Table I). In these cases no approximations of the kind used in Eqs. (A4) or (A5) really apply. However, all the results were still in keeping with Eq. (A5), that is to say the calculated Compton defects were so small as to be undetectable,  $\approx 5$  keV. It is important to emphasize that all the above applies only to the centroid of the quasi-Compton peak. Where this peak is not observable or significantly distorted due either to energy considerations or interference from the IRD (or both) the simple classical approach utilized above cannot be applied.

\*Work performed under the auspices of the U.S. Energy Research and Development Administration, W-7405-Ena-48.

†Now at Air Force Institute of Technology, Wright-Patterson Air Force Base, Ohio.

<sup>1</sup>M. Gavrilu, Phys. Rev. A **6**, 1348 (1972).

<sup>2</sup>L. A. Wittwer (private communication), available as UCRL 51268, 1972 (unpublished).

<sup>3</sup>J. H. Hubbell, W. J. Veigle, E. A. Briggs, R. T. Brown, D. T. Cromer, and R. J. Howerton, J. Phys. Chem. Ref. Data **4**, 471 (1975).

<sup>4</sup>J. Randles, Proc. Phys. Soc. Lond. A **70**, 337 (1957).

<sup>5</sup>M. Schumacher, Z. Phys. **242**, 444 (1971).

<sup>6</sup>D. Brini, E. Fuschini, N. T. Grimellini, and D. S. R. Murty, Nuovo Cimento **16**, 727 (1960).

<sup>7</sup>Z. Sujkowski and B. Nagel, Ark. Fys. **20**, 323 (1961).

<sup>8</sup>J. Varma and M. A. Eswaran, Phys. Rev. **127**, 1197 (1962).

<sup>9</sup>S. Shimizu, Y. Nakayama, and T. Mukoyama, Phys. Rev. **140**, 806 (1963).

<sup>10</sup>L. V. East and E. R. Lewis, Physica **44**, 595 (1969).

<sup>11</sup>S. N. Chintalapudi and K. Parthasaradhi, Indian J. Phys. **43**, 492 (1969).

<sup>12</sup>D. S. R. Murty, D. V. Krishan Reddy, and E. Narasimhacharyulu, Indian J. Pure Appl. Phys. **9**, 305 (1970).

<sup>13</sup>O. Pingot, J. Phys. (Paris) **33**, 189 (1972).

<sup>14</sup>J. W. Motz and G. Missoni, Phys. Rev. **124**, 1458 (1961).

<sup>15</sup>G. C. Spitale and S. D. Bloom, UCRL 52082, 1976 (unpublished).

<sup>16</sup>J. H. Neiler and P. R. Bell, *Alpha-, Beta-, and Gamma-Ray Spectroscopy*, edited by K. Siegbahn, (North-Holland, Amsterdam, 1965), p. 253.

<sup>17</sup>G. C. Spitale and S. D. Bloom (unpublished).

<sup>18</sup>W. C. Heitler, *The Quantum Theory of Radiation* (Oxford, Clarendon, 1954), pp. 176 and 333.

<sup>19</sup>J. M. Jauch and F. Rohrlich, *The Theory of Photons and Electrons* (Addison-Wesley, Reading, Mass., 1976), p. 229.

<sup>20</sup>F. Bloch, Phys. Rev. **46**, 674 (1934).

<sup>21</sup>R. D. Evans, Handb. Phys. **34**, 218 (1958).